Phthalocyanine photosensitizer in polyethylene glycol-block-poly(lactide-co-benzyl glycidyl ether) nanocarriers: Probing the contribution of aromatic donor-acceptor interactions in polymeric nanospheres

Gwenaelle E.N. Pound-Lana, Giani Martins Garcia, Izabel C. Trindade, Patricia Capelari-Oliveira, Thais Godinho Pontifice, José Mário Carneiro Vilela, Margareth Spangler Andrade, Benjamin Nottelet, Bruna B. Postacchini, Vanessa C.F. Mosqueira

Phthalocyanine photosensitizer in polyethylene glycol-*block*-poly(lactide-*co*-benzyl glycidyl ether) nanocarriers: Probing the contribution of aromatic donor-acceptor interactions in polymeric nanospheres

Gwenaelle E.N. Pound-Lana[a,*], Giani M. Garcia[a,1], Izabel C. Trindade[a,1],
Patrícia Capelari-Oliveira[a], Thais Godinho Pontifice[a], José Mário C. Vilela[b],
Margareth S. Andrade[b], Benjamin Nottelet[c], Bruna B. Postacchini[d], Vanessa C.F. Mosqueira[a,*]

[a] *Laboratory of Pharmaceutical Development and Nanobiotechnology, School of Pharmacy, Universidade Federal de Ouro Preto, Minas Gerais, Brazil*
[b] *CIT – Centro de Inovação e Tecnologia Senai-Fiemg, Avenida José Cândido da Silveira, 2000, Horto, Belo Horizonte 31035-536, Minas Gerais, Brazil*
[c] *Institut des Biomolécules Max Mousseron (IBMM) UMR 5247, Université Montpellier, CNRS, ENSCM, Montpellier, France*
[d] *Laboratory of Molecular Photophysics, Physics Department, Universidade Federal de Ouro Preto, Ouro Preto, Brazil*

ABSTRACT

Keywords:
Drug nanocarrier
Phthalocyanine
Photosensitizer
Biodegradable polymer
Amphiphilic block copolymer
Field flow fractionation

For best photosensitizer activity phthalocyanine dyes used in photodynamic therapy should be molecularly dispersed. Polyethylene glycol-*block*-polylactide derivatives presenting benzyl side-groups were synthesized to encapsulate a highly lipophilic phthalocyanine dye (AlClPc) and evaluate the effect of π-π interactions on the nanocarrier colloidal stability and dye dispersion. Copolymers with 0, 1, 2 and 6 mol% of benzyl glycidyl ether (BGE) were obtained via polyethylene glycol initiated ring-opening copolymerization of D,L-lactide with BGE. The block copolymers formed stable, monodisperse nanospheres with low in vitro cytotoxicity. AlClPc loading increased the nanosphere size and affected their colloidal stability. The photo-physical properties of the encapsulated dye, studied in batch and after separation by field flow fractionation, demonstrated the superiority of plain PEG-PLA over BGE-containing copolymers in maintaining the dye in its monomeric (non-aggregated) form in aqueous suspension. High dye encapsulation and sustained dye release suggest that these nanocarriers are good candidates for photodynamic therapy.

1. Introduction

The chloroaluminum phthalocyanine (AlClPc, Fig. 1) is a second generation photosensitizer currently under investigation in photodynamic therapy [1] and photoacoustic imaging [2]. Several metal phthalocyanines show cytotoxic behavior under laser light irradiation via reactive oxygen species production. Due to its low aqueous solubility AlClPc parenteral administration in animals and humans requires its association to a drug carrier [3]. Nanostructured formulations containing AlClPc have been reported, which include lipid-core polymeric nanocapsules [4–6], polymeric nanospheres (NS) [5], surfactant micelles [7], polymeric micelles [8], phospholipid vesicles [9], nanoemulsions [5,10] and solid lipid nanoparticles [11], among the most successful approaches. These differ in the amount of AlClPc loaded in the formulation, often expressed as payload, and in the ability of the photosensitizer to generate the cytotoxic reactive oxygen species. The degree of aggregation of the dye at its site of action is a crucial parameter and best photosensitizer effect is achieved when the dye is dispersed in its monomeric form [12].

Amphiphilic *block*-copolymers form supramolecular assemblies in aqueous medium with lipophilic compounds physically entrapped in a hydrophobic polymer matrix. These are valuable for the intravenous administration of low molecular weight chemotherapeutic and theranostic agents [13]. By carefully adjusting the physico-chemical
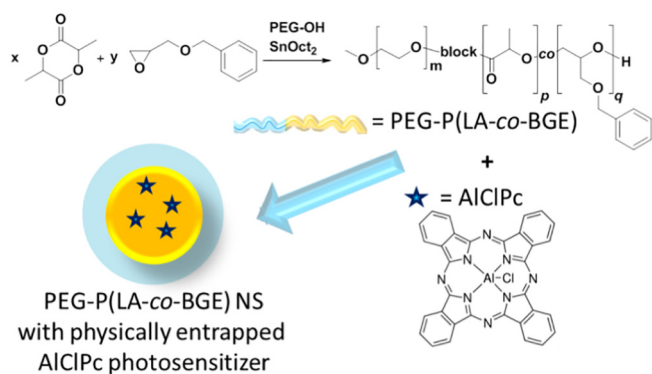
Fig. 1. General scheme for polyethylene glycol-*block*-poly(D,L-lactide-*co*-benzyl glycidyl ether) block copolymer synthesis and encapsulation of chloroaluminum phthalocyanine (AlClPc) in polymeric nanospheres (NS).

properties of each block with respect to the compound to encapsulate, stable nanoparticle dispersions can be achieved. Introducing aromatic groups along the polymer chain was found to improve the capacity of amphiphilic block copolymers in micelles to load hydrophobic aromatic compounds [14–18]. Benzoyl and naphthoyl groups were introduced along polymethacrylamide and increased the stability and capacity of the micelles to load paclitaxel and docetaxel [18]. In another study, aromatic π-π interactions between the polymer matrix and a porphyrin photosensitizer (Pheo) increased the loading capacity of the micelles and also reduced aggregation of the probe, thus enhancing the photodynamic properties [19]. In the case of polymeric micelles the introduction of lipophilic aromatic groups typically decreases the polymer critical micelle concentration and adds an enthalpic gain, which favors the stability of their self-assemblies with lipophilic compounds in aqueous medium. These results prompted us to evaluate the effect of aromatic side groups in polylactide (PLA) on the encapsulation efficiency and molecular dispersion of lipophilic compounds bearing aromatic groups in polymeric NS. However, polymeric NS differ from micelles because the latter are kinetically frozen structures and are generally not at thermodynamic equilibrium [20]. Consequently, the influence of π-π interactions between the polymer matrix in NS and an aromatic encapsulated drug or dye has not been established. In addition, by introducing aromatic benzyl groups along the hydrophobic polymer chain, in our case PLA, other physico-chemical properties may suffer alterations. Among these, the block copolymer purity, the hydrophilic/lipophilic balance, and T_g of the polymers, which may alter the size and colloidal stability of nanocarriers, the loading and release of hydrophobic compounds [21,22].

In order to probe the contribution of aromatic donor-acceptor interactions in core-shell polymeric NS derived from PEG-PLA, LA was copolymerized with benzyl glycidyl ether (BGE) in the presence of a polyethylene glycol (PEG) macro-initiator to produce block copolymers with variable amounts of BGE in the polymeric chain, identified as PEG-*block*-P(LA-*co*-BGE$_{x\%}$) (Fig. 1). In a recent publication we presented the copolymerization of LA with functional glycidyl ethers, including BGE, and showed preliminary results concerning the formation of block copolymers with PEG [23]. In the present work the block-copolymerization behavior was studied in further details. A series of four polymers were obtained from polymerization feed ratios of 0 to 46 mol% of BGE, characterized in terms of molar mass, molar mass distribution and co-monomer composition. In addition, a polymerization kinetic study was carried out using gel permeation chromatography (GPC) with refractive index and UV-absorption. The ability of the benzylated block copolymers to form stable nanoparticles loaded with the phthalocyanine dye AlClPc was evaluated and compared to the widely used PEG-PLA block copolymer. Photo-physical characterization of the dye within the polymeric NS was achieved by UV–Vis absorption and steady-state fluorescence spectroscopy. Dye encapsulation and release from the

nanoparticles in *n-octanol* and in cell culture medium supplemented with fetal bovine serum (FBS) was studied by HPLC-FLD and by AF4-MALS-FLD, respectively. The influence of a small proportion of BGE units in the mostly PEG-PLA block copolymer is discussed with respect to its ability to encapsulate, disperse and release AlClPc. Finally, the toxicity of the polymers in nanostructured form was evaluated via MTT cell viability assay on a J774.A1 macrophage-like cell line and on the non-phagocytic Vero cell line.

2. Experimental section

2.1. Materials

Aluminum phthalocyanine chloride (AlClPc, dye content 85%), benzyl glycidyl ether (BGE, 99%), monomethoxy polyethylene glycol (PEG$_{5k}$, DP = 113 by NMR), tin (II) 2-ethylhexanoate (SnOct$_2$, 95%), toluene (dry, 99%) 3-(4,5-ditmethylthiazol-2-yl)-2,5-diphenylte-trazolium bromide (MTT salt), dimethylsulfoxide (DMSO, ACS reagent grade), deuterated chloroform (CDCl$_3$), deuterated DMSO (DMSO-d_6) and tetrahydrofuran (THF, HPLC grade, with 250 ppm 3,5-di-tert-4-butylhydroxytoluene (BHT, 99%) added) purchased from Sigma-Aldrich and PA grade dichloromethane, hexane, propan-2-ol and acetone from VETEC (Brazil) were used without further purification. 3,6-Dimethyl-1,4-dioxane-2,5-dione (LA, 98%) was purified by three successive recrystallizations from dry toluene. Ultrapure water was obtained on a Symplicity-MilliQ system (Millipore, USA). Dulbecco's Modified Eagle Medium (DMEM, 4.5 g/L glucose and L-Glutamine), antibiotic solution (streptomycin 10 mg/mL + 10,000 I.U. of penicillin), 0.25% Trypsin-EDTA and phosphate-buffered saline (PBS) were purchased from Lonza (USA). Fetal bovine serum (FBS) was purchased from Cultilab (Brazil). Trypan Blue solution was purchased from LGC Biotecnologia (Brazil). American Type Culture Collection (ATCC, USA) Vero cells (normal epithelial cells from African green monkey kidney ATCC® CCL-81™) and J774A.1 (reticular sarcoma macrophages from *Mus musculus* mice, ATCC® TIB-67) were provided by Rio de Janeiro Cell Bank. The cells were cultured in DMEM supplemented with 10% FBS and 1% of antibiotic stock solution. The cells were incubated at 37 °C and 5% CO$_2$. Cells were subcultured until reaching 80% of confluency and detached with trypsin-EDTA or mechanically. Cells were counted on a Neubauer counting plate after labelling with trypan blue.

2.1.1. General procedures

The polymer composition was determined by ^{1}H NMR spectroscopy recorded on a Bruker AVANCE DRX400 MHz spectrometer. The samples were prepared at 60 mg/mL in CDCl$_3$ and the spectra recorded at 25 °C with a minimum of 64 transients. DOSY NMR experiments were recorded in DMSO-d_6 at 300 K on a Bruker Advance III spectrometer. The DOSY spectra were acquired with the dstebpgp3s pulse program from the Bruker topspin software, with 32 K time domain data points in the t2 dimension and 32 t1 increments. NMR data was processed using Bruker topspin software version 3.5. GPC was used to characterize the polymer molar mass, molar mass dispersity (Đ) and BGE content on an Agilent Technologies 1260 Infinity unit comprising a solvent degasser, isocratic pump, an Agilent 1260 Infinity UV detector (G1314F, detection wavelength 254 nm) and a differential refractive index detector (G1362A RID at 35 °C) in series, a Varian PLgel 5 μm MiniMix-D 50 × 4.6 mm pre-column and two Agilent PLgel 5 μm MiniMix-D 250 × 4.6 mm columns in series at 30 °C with HPLC grade THF with 250 ppm BHT stabilizer as the eluent at a flow of 0.25 mL/min. The samples were prepared at a concentration of 3 mg/mL in the eluent, filtered (0.22 μm PVDF Millipore filter) and the injection volume was 20 μL. A molar mass calibration was obtained using Agilent Technologies EasiVial narrow dispersion polystyrene standards (162–371,100 g·mol^{-1}) and a calibration for BGE content in the polymer, as described in Supplementary data. Fluorescence and UV–Vis absorption spectra were recorded on a RF-5301PC fluorescence

Table 1
Synthetic and characterization data of block copolymers of poly(lactide-co-benzyl glycidyl ethers) with monomethoxy polyethylene glycol.

Entry	Polymer code	mol% BGE in feed	Pol. time (min)	LA conv. (%)[a]	mol% BGE in pol.[b]	wt% PEG by NMR[b]	M_n by NMR (g/mol)[b]	M_n by GPC (g/mol), Đ [c]	T_m[d] (°C)/ΔHm (J/g)	T_g [e] (°C)
1	PEG-PLA	0	25	91	NA	20	25,500	19,800 *1.26*	50.5/28.9	ND
2	PEG-P(LA-co-BGE$_{1\%}$)	6	40	90	1.0	19	25,900	15,700 *1.24*	48.8/24.7	35
3	PEG-P(LA-co-BGE$_{2\%}$)	24	40	84	2.2	19	26,500	12,400 *1.25*	46.9/33.3	ND
4	NA	46	40	28	12	43	11,700	5800 *1.4*∗	ND	ND
5	PEG-P(LA-co-BGE$_{6\%}$)	46	150	73	5.8	23	21,400	9200 *1.29*	48.5/26.3	12

Experimental conditions: SnOct$_2$ ring-opening polymerization catalyst; macroinitiator: mPEG$_{5k}$, $T = 120$ °C, bulk; Molar ratios D,L-lactide:mPEG$_{5k}$:SnOct$_2$ = 140:1:1.1; [a] gravimetric; [b] by NMR; [c] by gel permeation chromatography; [d] melting temperature and enthalpy determined on first heating and [e] glass transition temperature determined on second heating by differential scanning calorimetry; ∗ trimodal. ND, not determined; NA, not applicable (the polymer was characterized but not used in NS); BGE benzyl glycidyl ether; PEG polyethylene glycol; NMR ^{1}H nuclear magnetic resonance; GPC gel permeation chromatography.

spectrophotometer (Shimadzu Scientific Instruments, Japan) and AJX-6100 PC (Micronal S.A., Brazil, SP) double beam spectrophotometer, respectively, in a 10 mm optical path quartz cuvette. Batch dynamic light scattering (DLS) and zeta potential analyses by electrophoretic light scattering were performed on a Zetasizer Nano ZS (Malvern Instrument, UK) instrument with a 633 nm He-Ne Laser. The polymeric NS suspensions (20 μL) were diluted in 1 mM aqueous NaCl (980 μL) and the Z-average hydrodynamic diameter (D_h) was determined from the 173° backscattered light intensity fluctuations via cumulant analysis with the Zetasizer 7.11 software (Malvern) using the Stokes-Einstein equation and values of 0.8872 cP (water viscosity) and 1.330 (water refractive index).

AF4 fractionation of the polymeric NS was performed on a Postnova analytics (Landsberg, Germany) AF2000 MT system comprising two PN1130 HPLC pumps (tip and focus pumps) and AF2000 module (crossflow pump), a PN5300 autosampler, PN4020 channel oven, and a separation channel fitted with a Postnova AF2000 MT Series NovaRC AQU 5 kDa cut-off regenerated cellulose membrane and a 350 μm spacer all under controlled temperature (25 or 37 °C). The fractionated sample was characterized using a PN3211 UV detector with absorbance at 254 nm, and a PN 3412 fluorescence detector with excitation at 650 and emission at 680 nm, unless otherwise indicated. The gyration diameter of each fraction was determined with a PN3621 multi-angle laser light scattering (MALS) detector with a 532 nm laser (20°–164°, 19 angles) and the hydrodynamic diameter with a Zetasizer Nano ZS (Malvern Instrument, UK – as described above), in series. The carrier liquid was 10 mM NaCl in Milli-Q water filtered on a 0.1 μm PTFE membrane filter (Millipore®). The NS suspensions were diluted at 1:5 in the carrier liquid or in DMEM/10%FBS. The detector flowrate was maintained at 0.5 mL/min; the injection flowrate was set at 0.2 mL/min with injection time of 1 min, an injection volume of 20 μL and a transition time of 1 min. An initial crossflow of 2.0 mL/min was applied during injection, maintained for 3 min, was set to decrease exponentially to 0.05 mL/min over a period of 15 min, maintained at 0.05 mL/min for 25 min, and kept at 0 mL/min for 8 min allowing complete elution of the sample. The gyration diameters (D_g) were determined for each fraction at 3.8 s time intervals using the angular variation of the scattered light intensity at angles 20°–164° (19 angles) recorded on the MALS detector using the Postnova AF2000 software calculation for spherical shape model, and D_h at 5.0 s intervals. For AFM analysis a 10 μL sample of the NS suspension was deposited on freshly cleaved mica, dried under a flow of argon and the AFM images were acquired in air at room temperature on a Dimension 3000 equipment monitored by a Nanoscope IIIa controller (Digital Instruments, Santa Barbara, CA, USA).

2.1.2. Calculation of the polymer composition by NMR

The spectrum intensity was normalized by attributing to the methyl proton signal integral of the PEG$_{5k}$ terminal group (3.36 ppm, CH_3-O, 3H) the value of 3. The polymer content in BGE with respect to lactide (in mol%) was calculated using the integral of the aromatic proton signal (7.2–7.4 ppm, CH_{Ar}, 5H, corrected for the residual solvent peak CHCl$_3$, 7.26 ppm, $I_{7.26} = 4.6$ determined on the PEG-*block*-PLA polymer) divided by 5 and the integral of the LA methine protons (5.0–5.3 ppm, $2 \times$ CH(CH$_3$) corrected for the overlapping methylene signal of BGE), divided by two, in percentage, as follows:

$$\text{mol\%BGE} = [(I_{7.2-7.4} - 4.6)/5]/\{(I_{7.2-7.4} - 4.6)/5 + [(I_{5.0-5.3} - (I_{7.2-7.4} - 4.6)/5)]/2\} \times 100$$

The copolymer molar mass ($M_{n,NMR}$) was calculated as the sum of the molar mass of the P(LA-co-BGE) block and PEG block as follows:

$$M_n, \text{NMR} = DP_{LA} \times MM_{LA} + DP_{BGE} \times MM_{BGE} + DP_{PEG} \times MM_{PEG}$$
$$= \{[I_{5.0-5.3} - (I_{7.2-7.4} - 4.6)/5]/2\} \times 144$$
$$+ [(I_{7.2-7.4} - 4.6)/5] \times 164$$
$$+ \{I_{3.51-3.75} - [(I_{7.2-7.4} - 4.6)/5] \times 4\}/4 \times 44$$

2.1.3. Polymer synthesis

PEG$_{5k}$ (0.373 g, 7.4×10^{-2} mmol) was weighed in an oven-dried 50 mL round-bottom flask, dry toluene (10 mL) was added to dissolve and dry PEG$_{5k}$ at 40 °C by azeotropic distillation under reduced pressure (repeated twice). SnOct$_2$ (26 μL, 8.2×10^{-2} mmol) and BGE (0, 111, 552 or 1391 μL, 0, 0.7, 3.2 or 8.7 mmol, for 0%, 6%, 24% and 46% BGE feed mol%, respectively) was added, the mixture was dissolved in dry toluene (5 mL) and toluene was evaporated under reduced pressure. Freshly recrystallized LA (1.50 g, 10.4 mmol) was added, the flask was fitted with a magnetic stir-bar and a vacuum adapter, purged with five cycles of vacuum/argon gas, sealed and placed in a heated oil bath for a temperature inside the flask of 120 °C. Polymerization was allowed to proceed under 360 rpm magnetic stirring for 25, 40 or 150 min, as indicated in Table 1. The polymerization mixture was dissolved in dichloromethane (8 mL), the polymer was recovered by precipitation in hexane (80 mL), re-dissolved in dichloromethane (8 mL), precipitated in isopropyl alcohol (80 mL), washed with diethyl ether (2 × 10 mL) and dried under high vacuum for 24 h.

2.2. Polymerization kinetic study

The polymerization flask was prepared as described above for a feed BGE content of 24 mol%. Following the vacuum/argon gas purge the flask was fitted with a rubber septum and dry, degassed toluene (3.0 mL) was introduced via a stainless steel needle through the septum.
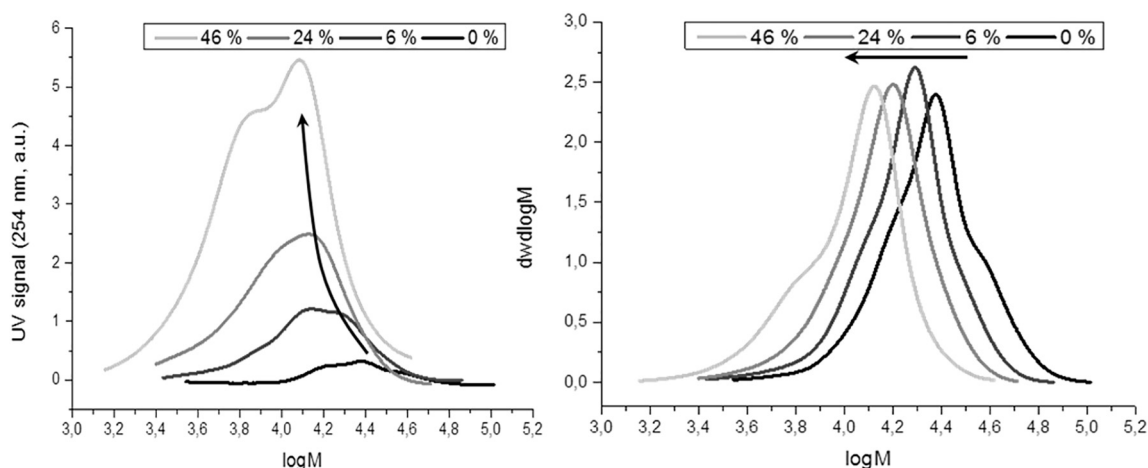
Fig. 2. Molar mass distributions of the polymers by gel permeation chromatography with UV absorption at 254 nm (left) and refractive index detection (right). 0, 6, 24 and 46% correspond to the mol% of BGE with respect to the total monomer content in the polymerization feed. Further polymer characterization data is available in Table 1.

The flask was placed in a heated oil bath for a temperature inside the flask of 110 °C. At repeated time intervals a polymerization sample (approx. 0.2 mL) was withdrawn with a syringe fitted with a dry stainless steel needle at 60 °C (to avoid polymer precipitation in the needle), weighed in a glass vial and THF with glacial acetic acid (3.0 mL of a solution at 8.3 mM) was added to quench the polymerization and prepare the sample for GPC characterization. The polymer BGE content was determined as described in Supplementary data.

2.3. NS preparation

The polymer (20 mg) was dissolved in acetone (4.0 mL) and AlClPc (1.0 mg/mL in ethanol, 200, 100, 50, 25 or 13 μL) was added. The resulting solution was poured through a plastic syringe into 8.0 mL of ultrapure water under magnetic stirring, maintained under stirring for 10 min and concentrated under reduced pressure at 25 °C to a final volume of 2 mL (polymer concentration: 10 mg/mL, AlClPc: 100, 50, 25, 13 or 6 μg/mL, respectively).

2.4. AlClPc encapsulation and in vitro release

The total AlClPc in the colloidal suspension was determined before and after filtration using a 0.8 μm filter (Durapore, Millipore®). The NS suspension (100 μL) was added to 1.9 mL of acetonitrile (to disrupt the NS and release AlClPc), vortex-mixed for 5 min, and centrifuged at 500 ×g for 30 min. The total AlClPc in the colloidal suspension was determined in the supernatant by HPLC-FLD, using a previously described method [4] with a mobile phase composed of methanol:acetone:dimethylformamide 80:15:5 (v/v). Another 400 μL of the filtrate were submitted to ultrafiltration in an AMICOM device (Microcon Ultrafilter, MWCO 50,000 Da, Millipore®) at 500 ×g for 60 min to separate AlClPc associated with nanostructures from free AlClPc (non-encapsulated). AlClPc associated with the nanostructures was retained in the upper compartment of the device. Acetonitrile (150 μL) was added to 50 μL of the ultrafiltrate and the sample submitted to HPLC-FLD for the quantification of the non-encapsulated AlClPc (free AlClPc). All samples were filtered using a 0.45 μm filter and 25 μL were injected in the HPLC-FLD system. The analyses were performed in triplicate. The percentage of AlClPc-loading in the NS was calculated as the difference between the total AlClPc in the colloidal suspension and the free AlClPc in the aqueous phase divided by the total AlClPc in the colloidal suspension, in percentage. AlClPc release from the NS suspension in *n-octanol* was performed under sink conditions, as previously described [5,24]. Briefly, 0.5 mL of NS suspension prepared at AlClPc loading of

25 μg/mL were placed in a centrifuge tube with 1.5 mL of *n-octanol*, in triplicate. The tubes were incubated at 37 °C on a mechanical shaker. At predetermined time intervals, the tubes were centrifuged at 500 ×g for 1 min. A sample of the organic layer was withdrawn (100 μL) and diluted in 900 μL of acetonitrile. The amount of drug released was determined by HPLC-FLD [4].

2.5. Cytotoxicity of blank NS on J774A.1 and Vero cells

The cytotoxicity of NS was determined by MTT test adapted from Mosmann [25]. Cells were plated at a density of 2.4×10^4 and 3.0×10^3 J774A.1 and Vero cells per well, respectively, on 96-well plates in complete culture medium (200 μL per well) and incubated for 24 h for adhesion. Cells were exposed to different concentrations of NS (0, 10, 50, 100, 500, 1000 μg/mL) for 24 h. The culture medium containing NS was removed and the cells were washed twice to remove NS residues with PBS containing Ca^{2+} and Mg^{2+} to prevent cell detachment. Culture medium containing MTT (0.5 mg/mL, 200 μL) was added and the plates were incubated for an additional 4 h at 37 °C. In addition, the NS were pre-incubated with MTT in culture medium for 4 h at 37 °C to evaluate a possible interaction of the nanoparticles in the reduction of this reagent. The plates were centrifuged at 400 ×g for 5 min, the medium was carefully removed and the formazan crystals were solubilized in DMSO (200 μL per well) at 37 °C. After complete dissolution of formazan crystals verified by optical microscopy, the absorbance of each well was measured at 570 and 650 nm (reference) on a Microplate Reader Emax (Molecular Devices, USA). Cell viability was expressed in percentage relative to controls (cells not exposed to NS).

3. Results and discussion

3.1. Synthesis and characterization of block copolymers

Copolymers were obtained from a monomethoxy-PEG macro-initiator via tin octanoate catalyzed ring-opening copolymerization of LA with BGE at feed ratios of 0 to 46 mol% BGE with respect to LA (Table 1). Throughout the manuscript these polymers are referred to as PEG-P(LA-*co*-BGE$_{x\%}$) where x indicates the mol% of BGE with respect to the total comonomer in the P(LA-*co*-BGE) block. Incorporation of the BGE comonomer in the polymer was evidenced by GPC with UV detection (Fig. 2). An increase in the UV signal with increasing feed molar ratio of BGE was observed, corresponding to the incorporation of benzyl groups in the copolymer.

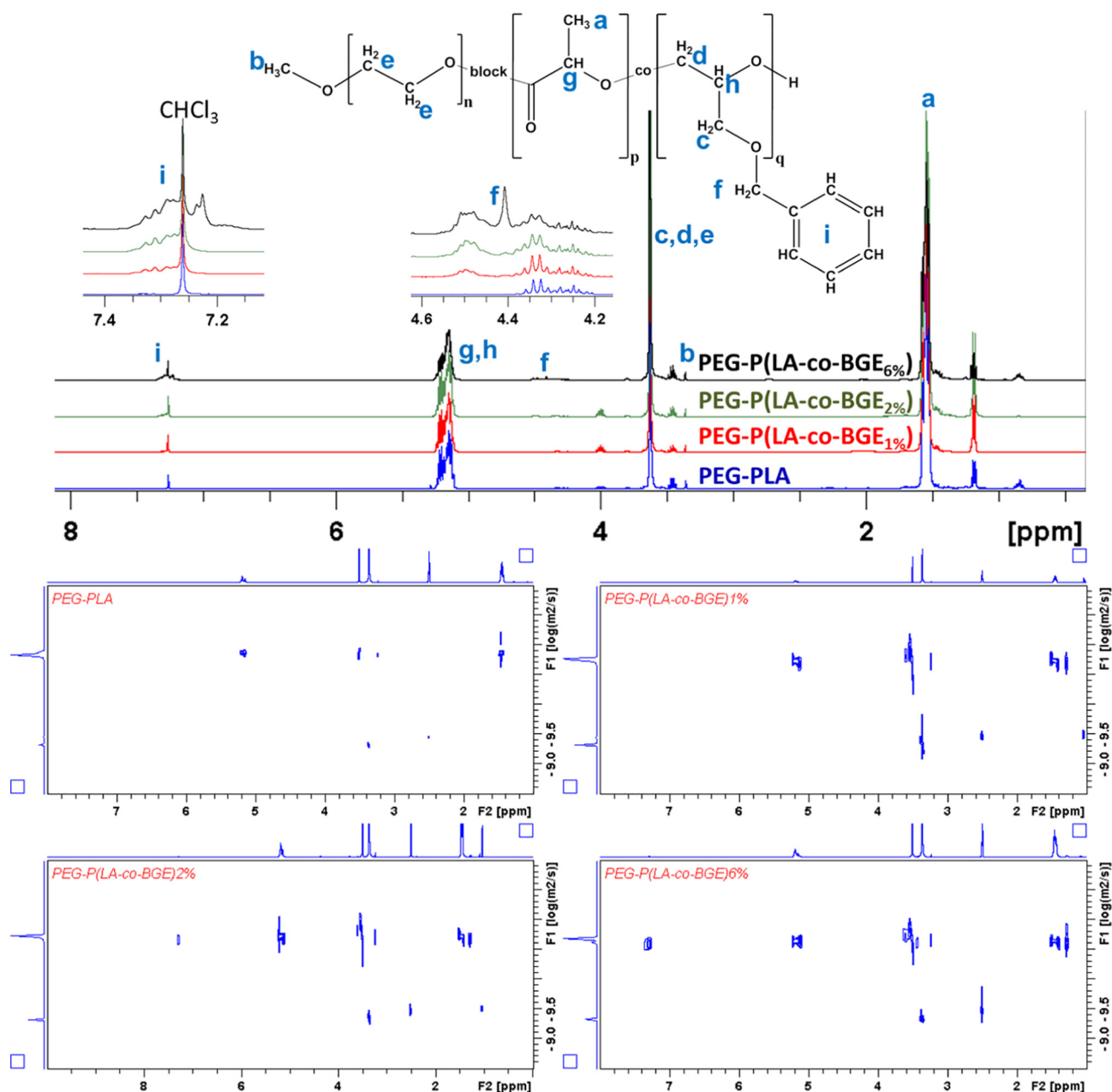The polymer composition was determined by ^{1}H NMR spectroscopy

Fig. 3. ^{1}H NMR (top) and 2D-DOSY-NMR (bottom) spectra of the copolymers.

(Fig. 3), with the help of previously reported peak assignments [23,26]. The PEG content in the copolymer determined by NMR (Table 1) was similar after isolation of the polymer by precipitation (19–23 wt%, depending on monomer conversion, Table 1 entries 1–3 and 5) as in the feed content (20 wt%), except for entry 4. Considering that polymer purification was carried out to remove pure PEG, maintenance of the PEG weight ratio in the copolymerization product indicates that all PEG chains were incorporated in the copolymer. In the case of entry 4, which had the highest feed content in BGE, low conversion was obtained in 40 min, resulting in a higher weight percent of PEG in the copolymer. By increasing the polymerization time to 150 min higher conversion was achieved and a polymer was obtained with similar PEG content to the feed composition.

The copolymer molar mass by GPC was lower than the value calculated by NMR. As the value calculated by NMR relies on the assumption that all chains are composed of one PEG block and one P(LA-co-BGE) block (see section 2.1.2 for calculation details), the lower value obtained by GPC suggests that not all chains had a PEG block. In addition, the higher the BGE feed content, the lower the copolymer molar mass by GPC, suggesting that BGE may provide a source of chain-initiating moieties. Similar observations were made in the previously reported copolymerization of LA with BGE [23]. The copolymers were further characterized via DOSY-NMR spectroscopy to evaluate the composition homogeneity. The DOSY spectra of the copolymers with 2 and 6% BGE show similar diffusion coefficients for BGE, LA and PEG signals (Fig. 3), indicating that the copolymers are composed of all three comonomers. The low sensitivity of the method did not allow further identification of chains lacking one or more of these comonomers nor characterization of the polymeric aromatic signal in the polymer comprising 1% BGE. Therefore, further characterization was carried out by GPC.

The polymeric UV peak area by GPC was proportional to the polymer content in BGE as determined by ^{1}H NMR spectroscopy (Supporting information). Therefore, it was possible to perform a
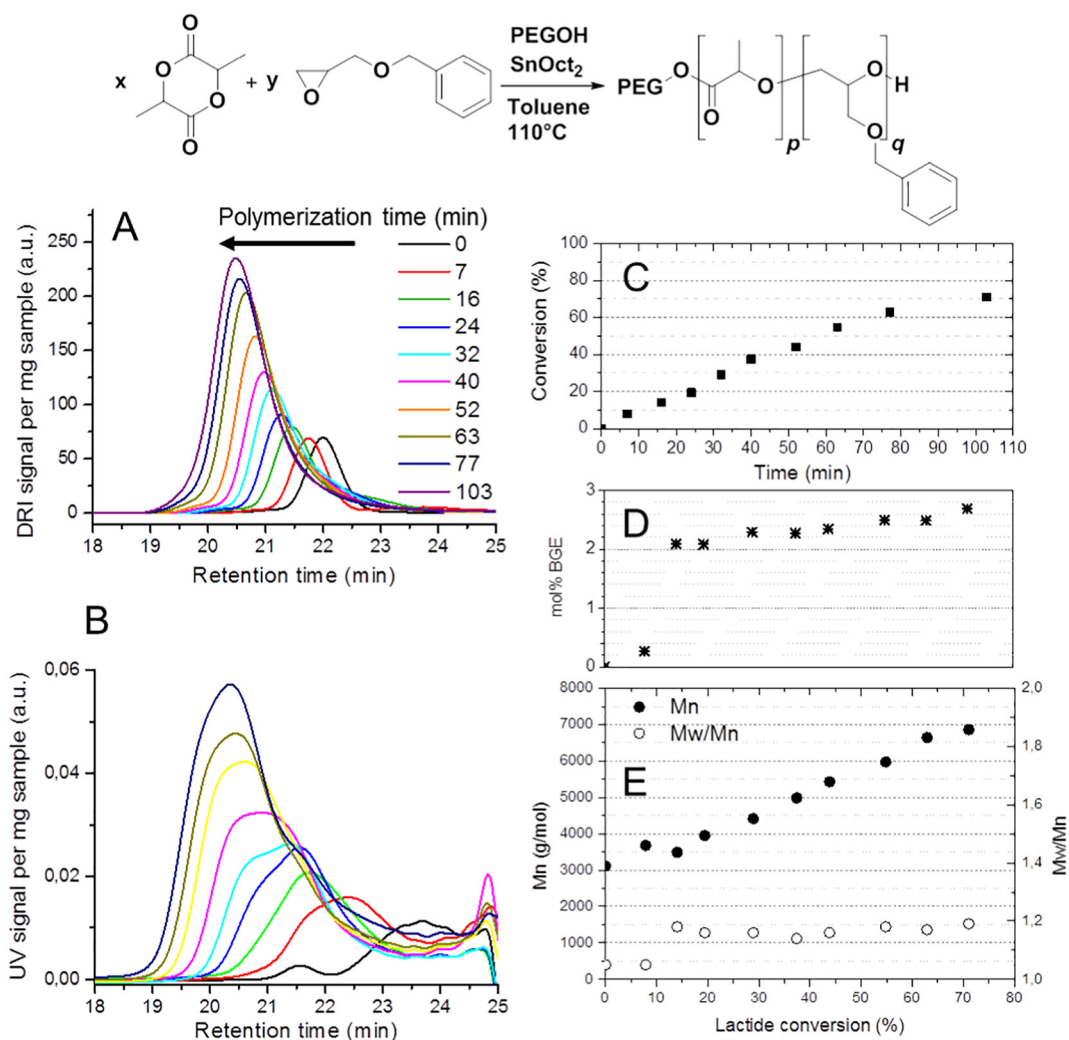
Fig. 4. Kinetic study of block copolymerization by gel permeation chromatography (GPC). D,L-Lactide (LA) was copolymerized with benzyl glycidyl ether (BGE) with mPEG$_{2k}$ as the macroinitiator and SnOct$_2$ as the catalyst at feed molar ratios of 140:44:1:1.1 (24 mol% BGE), in toluene (LA:toluene 1:2, w/v at 110 °C (Top scheme). Samples were withdrawn at polymerization times indicated on Fig. A and characterized by GPC with refractive index detection (A) and UV (254 nm) absorption (B) enabling the construction of Fig. C–E.

copolymerization kinetic study where the copolymer BGE content and molar mass distribution were characterized by GPC analysis of raw samples withdrawn from the polymerization mixture (Fig. 4). The polymerization conditions were adapted to allow sample withdrawal via an argon gas purged syringe. For this purpose the polymerization was carried out in solution in toluene at 110 °C instead of bulk at 120 °C. In addition, PEG$_{2k}$ was used instead of PEG$_{5k}$ to allow characterization of the macroinitiator and of the first samples by GPC, as PEG$_{5k}$ did not dissolve in the GPC eluent (THF). The PEG macroinitiator distribution shifted to higher molar masses already in the first sample (Fig. 4A), demonstrating the absence of polymerization inhibition mechanism. The molar mass increased with time and with conversion in a linear fashion up to 63% LA conversion. The last sample at 72% conversion seems to indicate a deviation from linearity. Nonetheless, all molar masses by GPC were dramatically lower than expected, suggesting that the monomer was distributed over a larger number of chains than those initiated by PEG. Additional information can be drawn from Fig. 4 regarding side-reactions in the copolymerization of LA with BGE and block copolymer formation. Firstly, a low molar mass distribution can be identified from the second sample at < 10% LA conversion. It has significant UV absorption but is hardly visible by RI detection (Fig. 4A and B, retention times 22.5–24.5 min), indicating that it consists of benzyl-rich species. This observation provides further

evidence that BGE-derived species compete with PEG in chain-initiation, whether in toluene (Fig. 4) or in bulk (Supporting information Fig. S2). Although the BGE-initiated distribution increases in molar mass with conversion and rapidly overlaps with the main polymer distribution visible by both UV and RI detection, a low molar mass tail is observed in all samples, suggesting that more chains are initiated throughout the polymerization process. The consequence is a decrease in the average molar mass of the polymer, as also observed in the polymers prepared in bulk at 120 °C (Table 1), and the presence of chains that do not contain a PEG block. The study in Fig. 4 therefore supports competing initiation by BGE-derived species as a contributor to polymer heterogeneity in terms of co-monomer sequence and molar mass. Finally, the mol% of BGE per chain (Fig. 4D) increased rapidly from 0 to 2.1 mol% from 0 to 14% LA conversion and then followed a steady although limited increase with conversion up to 2.7 mol%. The increase in BGE incorporation with conversion can be explained by the lower reactivity of BGE compared to LA. At high LA conversion its low concentration in the reaction medium favors BGE incorporation. The fact that the last sample had only 0.6 mol% more BGE than the sample at low conversion indicates that BGE homopropagation is not favored under our experimental conditions and that no long poly(BGE) segment would be present in the copolymers. In terms of polymerization conditions, as the size-distribution was significantly narrower and M$_n$
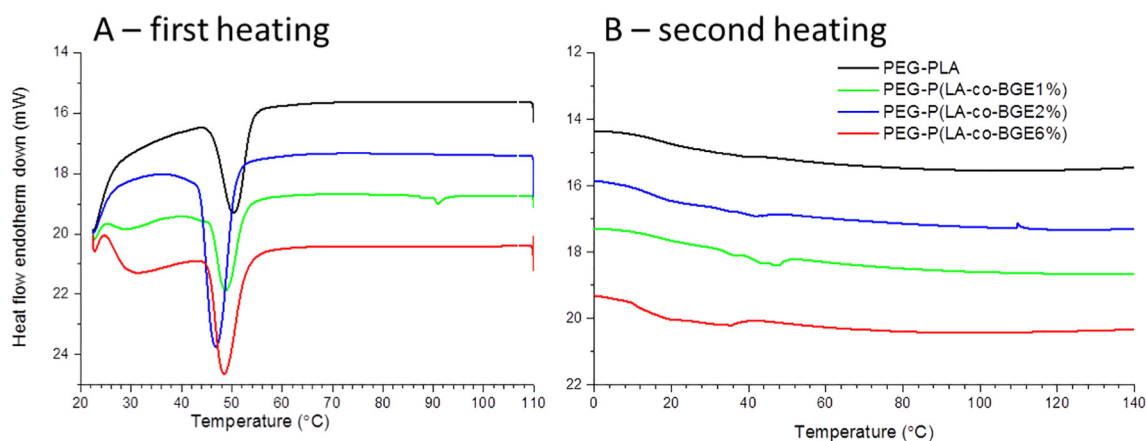
Fig. 5. Differential scanning calorimetry thermograms of the polymers at first heating (A) and second heating after thermal quenching (B).

closer to theoretical values in bulk at 120 °C than in toluene at 110 °C, the former conditions were selected to produce well-defined polymers used in NS preparation.

DSC analyses indicated a semi-crystalline behavior of the block copolymers in the bulk material (Fig. 5 and Table 1). A single endothermic melting peak was obtained in the first heating step, with onset at approximately 45 °C, corresponding to melting of the PEG_{5k} block. The presence of BGE in the PLA block did not prevent crystallization of the PEG_{5k} block, as already observed in block copolymers of PEG and PLA modified with a hydrophobic moiety [27]. The glass transition temperature (T_g) could not be determined unambiguously for all our samples. Thermal events were observed between 10 and 50 °C, which could correspond to glass transition of lactide-rich segments, typically in this temperature range. Solarski and coworkers pointed out that PLA presents a chain-relaxation event immediately after glass transition, which makes the determination of T_g difficult by conventional DSC [28]. Increasing amounts of BGE comonomer were expected to result in a decrease in T_g, as already observed in a BGE-CO_2 polycarbonate copolymer [29]. This occurs because the bulky and flexible benzyl ether side-chains increase the free volume in the copolymers. Polymer T_g above ambient temperature and an amorphous character of the core-forming polymer has been found to have a positive effect on drug loading of hydrophobic compounds within NS and on the release profiles of the nanoparticles [21,22].

3.2. Nanoparticle preparation and encapsulation of AlClPc

The ability of the block copolymers to form stable assemblies in aqueous medium was examined by preparing blank NS by the nanoprecipitation method [30]. All blank NS showed colloidal stability (no precipitation) for at least 45 days and average hydrodynamic diameters between 63 and 114 nm by DLS (Fig. 6). A clear trend was observed indicating an increase in nanoparticle size and decrease in colloidal stability with increasing BGE content in the copolymer (Fig. 6). In contrast, AlClPc-loaded NS remained stable for a minimum of 45 days only in the case of PEG-PLA NS and were generally larger than their blank counterparts. AFM images of NS containing AlClPc show discrete spherical nanoparticles for all NS (Fig. 7), very low polydispersity for PEG-PLA NS and some aggregation in NS from the polymers containing BGE. With 2 mol% BGE in the copolymer the NS containing AlClPc presented a blue precipitate on day 10 and at 6 mol% BGE on day 2. This precipitate could be resuspended by mild mechanical shaking, suggesting that it was formed by sedimentation of large particles. The zeta potential values of the various NS remained in the same range (−7 to −14 mV), with no significant changes with respect to polymer composition or AlClPc loading, and in agreement with polyester NS possessing a dense PEG surface coating [31].
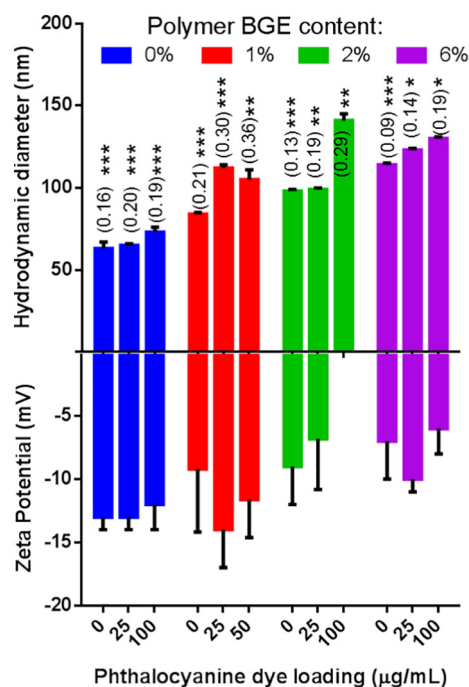

Fig. 6. Size and zeta potential of the phthalocyanine dye-loaded nanospheres. Phthalocyanine concentration in nanosphere suspensions in water at 10 mg of PEG_{5k}-*block*-P(LA-*co*-$BGE_{x\%}$)/mL; diameter and zeta potential values are averages of three measurements; values between brackets are polydispersity index; error bars are standard deviation; macroscopic stability (*** > 45 days, ** < 10 days, * < 2 days) was assessed through visual observation of the presence of precipitate on days 0, 1, 2, 10 and 45. The encapsulation efficiency determined at dye loading of 25 µg/mL was > 98% by HPLC for all NS.

The nanoprecipitation method is known to produce NS from PEG-*block*-polyester copolymers with a solid polyester core and a hydrated PEG corona [32]. The prolonged colloidal stability of the blank PEG-PLA NS and ability of AlClPc-loaded NS to remain stable at higher AlClPc loading compared to the other NS is attributed to the copolymer composition, and how it affected the NS size and PEG surface coverage, as discussed in the following paragraph. Self-assembly of pure PEG_{5k}-PLA block copolymers with PLA up to 30 kg/mol via the nanoprecipitation method is similar to non-equilibrium micelle-formation [33]. In this case the aggregation number, which is the number of polymer chains per nanostructure, and thus the size of the NS are governed by the relative size of each block, whereby a larger PLA block in PEG_{5k}-PLA copolymers lead to larger NS [33,34]. In this study all NS had the same PEG_{5k} content (approx. 20 wt%), but as the BGE content increased
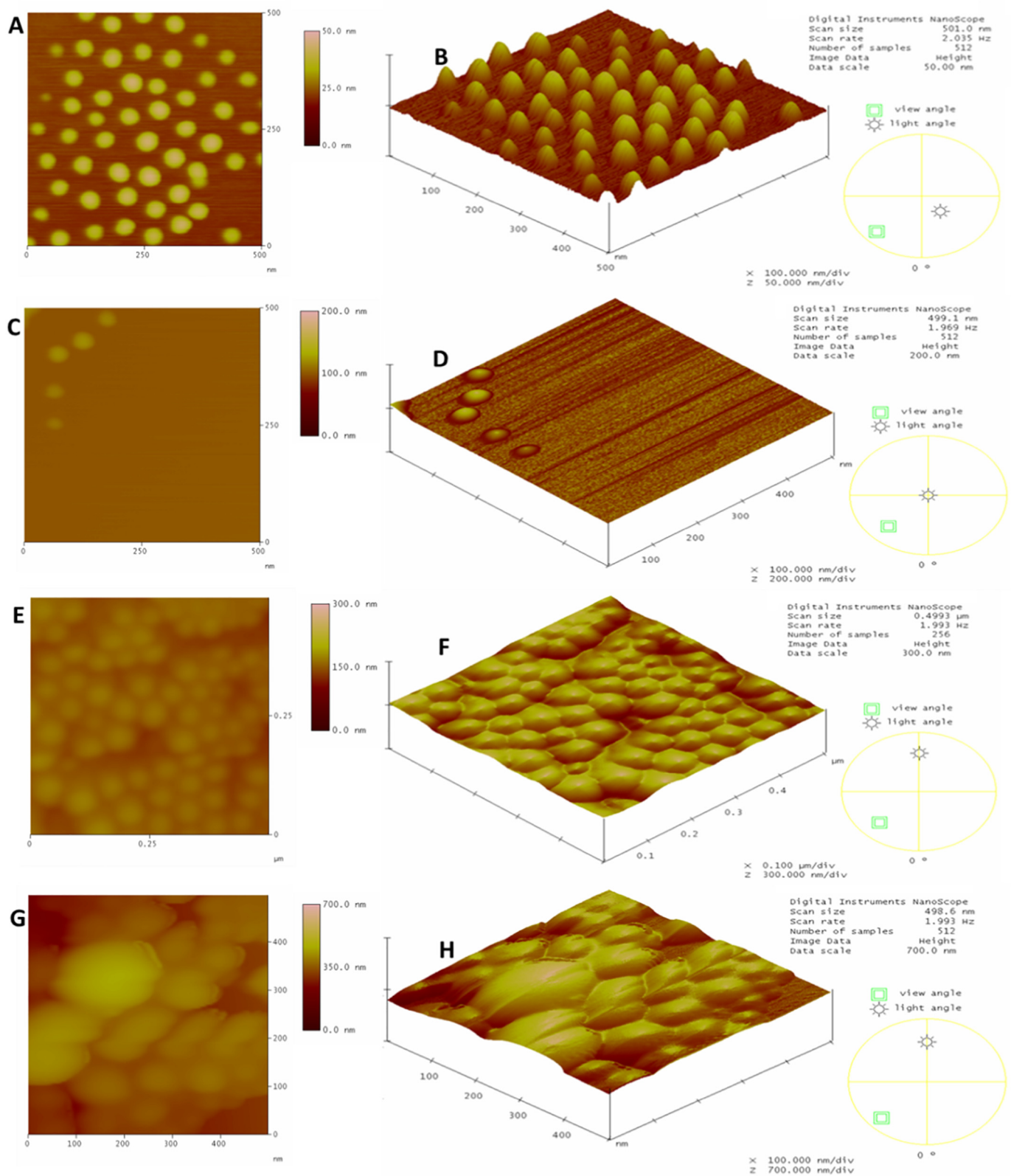
Fig. 7. Atomic force microscopy images of phthalocyanine loaded NS. The NS were loaded with AlClPc (25 μg/mL) in 10 mg/mL of PEG-PLA (A and B), PEG-P(LA-*co*-BGE$_{1\%}$) (C and D), PEG-P(LA-*co*-BGE$_{2\%}$) (E and F) and PEG-P(LA-*co*-BGE$_{6\%}$) (G and H). Height images (A, C and E) and three-dimensional view (B, D and F). Scan size: 500 × 500 nm.

the total polymer molar mass decreased (Table 1), and an increase in NS diameter was observed. Previous studies reported larger NS sizes than expected from the micellar aggregation model due to contamination of the block copolymers with PLA homopolymer as a consequence of poor control over the polymerization process [34] or to deliberate blending of homo and block-copolymers [23,35]. We tested this hypothesis by preparing NS from a blend of PLA_{9k} and $PEG_{5k}PLA_{15k}$ (40:60 w/w) and although we observed an increase in diameter from 63 nm (Fig. 6) to 72 nm (data not shown), it was significantly lower than the 35 nm diameter increase observed between NS of PEG-PLA and NS of PEG-P(LA-*co*-$BGE_{2\%}$) (Fig. 6). It is therefore likely that the larger size of BGE containing NS was due to the changes in chemical composition of the copolymers, in particular the hydrophilic/lipophilic balance between PEG and the P(LA-*co*-BGE) block. Several studies demonstrate the dependence of pegylated NS stability on the density of the PEG outer layer [36,37]. For a given PEG mass fraction in the copolymer, the PEG surface coverage will be lower on larger particles, leading to poorer steric hindrance between the particles and their aggregation [34].

While all blank NS suspensions were stable for up to 45 days, AlClPc loading dramatically reduced the stability of the NS from BGE containing copolymers (Fig. 6). Together with a further increase in NS size upon AlClPc loading, this data suggests that the NS hydrophilic/lipophilic balance was tipped to a thermodynamically unfavorable point leading to NP aggregation at high AlClPc loading. Substitution of LA units with BGE units in the copolymer increases the lipophilicity of the hydrophobic core-forming block. This can be empirically evaluated by calculating the *n-octanol*/water partition coefficient (CLogP). CLogP calculations using the Molinspiration cheminformatics software [38], indicate that the substitution of two LA units by two BGE units increases the logP value from 9.4 to 9.8, for a 3.6 kg/mol chain (see Supplementary data). Previous studies comparing the PEG chain-length requirements for colloidal stability with respect to the hydrophobicity of the core-forming block suggest that a longer PEG block or a higher ratio of PEG to P(LA-*co*-BGE) may be required to guarantee colloidal stability of the more hydrophobic AlClPc-loaded PEG-P(LA-*co*-BGE) NS [36].
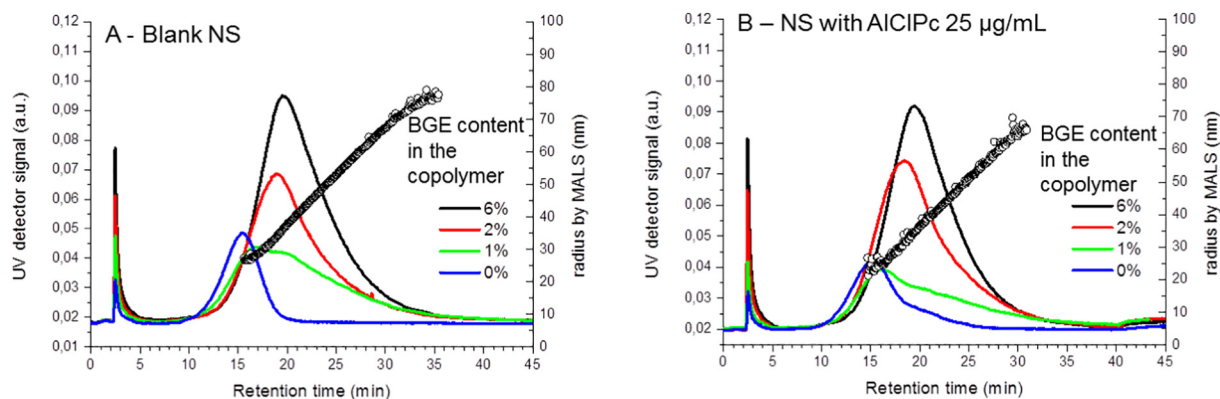
Further characterization of the NS size-distribution was carried out by AF4 (Fig. 8A and B). The concentration detector on our system is a UV–Vis absorption detector set at 254 nm and consequently the fractograms show a higher signal with increasing BGE content in the NS polymeric matrix due to a stronger absorption by benzyl rings in PEG-P(LA-*co*-BGE) compared to PEG-PLA. All samples had a monomodal narrow distribution with gyration diameters by MALS ranging from 20 to 160 nm and showed only a slight increase in size upon loading of AlClPc at 25 μg/mL. This size-range, well below 300 nm, makes the NS suitable for intravenous administration. Blank and AlClPc-loaded PEG-PLA NS had an upper-size limit of 80 and 110 nm, respectively, significantly lower than the other NS, in agreement with the AFM and batch DLS analyses.

3.3. Photophysical characterization of the NS containing AlClPc

In order to determine the aggregation state of the encapsulated dye the AlClPc-loaded NS were characterized for their UV–Vis absorption and fluorescence properties in colloidal suspension and compared to the dye in organic and in aqueous medium. Intense absorption bands are obtained for AlClPc in acetonitrile at 348 and 676 nm, with maximum absorption at 676 nm. These bands correspond to the B (or Soret) and Q_I bands, related to transition from the ground state to the second and first excited electronic state, respectively, of AlClPc in its monomeric form in organic solvent [39]. Less intense Q_{III} and Q_{II} bands appear at 610 and 644 nm, respectively. Phthalocyanine dyes, including AlClPc, display changes in their photophysical properties depending on the hydrophilic/lipophilic balance of their environments [39]. This is mostly due to their dimerization and further aggregation in poor solvents. Jayme observed a deviation from linearity in the Beer-Lambert equation of AlClPc in aqueous systems ($> 60\%$ water in water/ethanol mixtures) from concentrations as low as 0.15 μg/mL, and a shift in the absorption bands to higher wavelengths (390, 580 and 820 nm), attributed to the formation of J-type aggregates [40], as confirmed in the absorption spectrum of AlClPc in water (Fig. 9A). For AlClPc in PEG-PLA NS in aqueous suspension an absorption spectrum was obtained with very similar profile and intensity to that of free AlClPc in acetonitrile solution (Fig. 9B), indicating good dispersion of the dye within PEG-PLA NS colloids. In contrast, a sharp decrease in the intensity of the Soret band was observed with AlClPc loaded at the same content in NS prepared from copolymers containing 2 and 6% of BGE (Fig. 9B). Upon solubilizing these NS in acetonitrile a very similar spectrum to AlClPc in solution was obtained (not shown), indicating that the loss in absorption at 676 nm was reversible and was not due to degradation of the dye but to its environment affecting its photophysical behavior. This indicates that the polymer rich in benzyl groups created an environment less favorable to AlClPc molecular dispersion, however the spectra do not provide information as to whether the dye was present in an aggregated form associated to the NS or in the aqueous phase. Therefore, while PEG-PLA NS were able to prevent the formation of J-type AlClPc aggregates at concentrations up to 100 μg/mL, the polymers containing BGE were less efficient in dispersing the dye. By decreasing the payload to 25 μg/mL, fairly similar absorption intensities were obtained for NS composed of polymers with 0, 1 and 2% BGE, and slightly lower (approx. loss of 40% in absorption intensity at 676 nm) with the copolymer containing 6% BGE (Fig. 9C), suggesting a dye-loading dependent aggregation profile.

The fluorescence spectra of AlClPc in solution in acetonitrile present a red-shift in fluorescence emission upon an increase in concentration

Fig. 8. Size characterization of the nanospheres (NS) by asymmetric flow field flow fractionation. Fractograms of the NS suspensions prepared from polymers containing 0,1,2 and 6% benzyl glycidyl ether (BGE) diluted in the eluent 10 mM NaCl (aq) (1:5 v/v) were obtained at 25 °C with UV detection (254 nm). (○) gyration radius calculated by multi-angle light scattering (MALS) for the NS composed of PEG-P(LA-co-$BGE_{6\%}$).
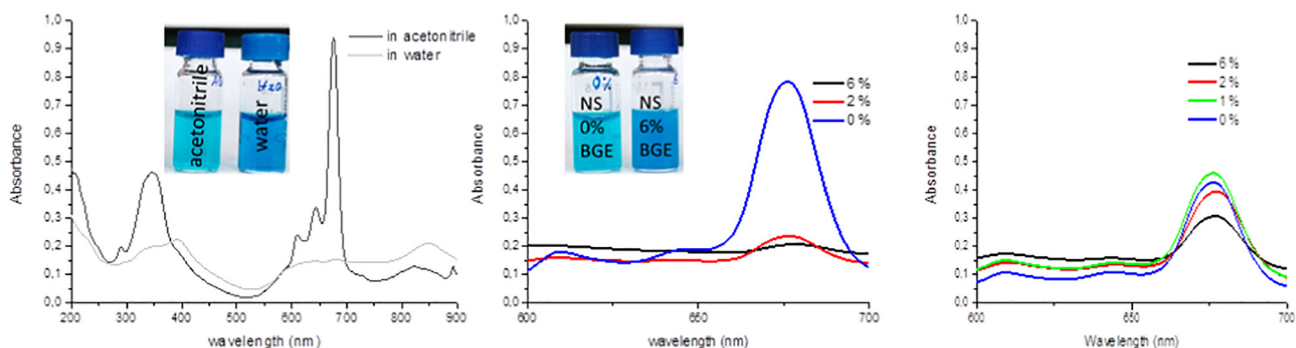
Fig. 9. UV–Visible absorption spectra of chloroaluminum phthalocyanine (AlClPc) in solution (A) in aqueous suspensions (B and C) of polymeric nanosphere (NS) composed of polyethylene glycol-*block*-poly(lactide-*co*-benzyl glycidyl ether) (PEG-*block*-P(LA-*co*-BGE)). 0, 1, 2 and 6% indicate the BGE mol% in the P(LA-*co*-BGE) block. Inserts: photographs of the solutions and NS suspensions at 100 μg of AlClPc/mL.

(Fig. 10A). This bathochromic shift has been attributed to reabsorption of the emitted photons by AlClPc molecules in the ground state, the so-called inner filter effect or self-quenching [41]. In aqueous suspension, an increase in AlClPc loading in PEG-PLA NS from 6 to 13 μg/mL resulted in an increase in fluorescence emission (Fig. 10B). At 25 μg/mL the fluorescence emission was similar to that at 13 μg/mL and further

increase in loading resulted in a decrease in fluorescence emission and a similar bathochromic shift from 680 to 688 nm, as observed for the dye in acetonitrile. This suggests that fluorescence quenching related to the inner filter effect occurred with an onset at AlClPc loading between 13 and 25 μg/mL in PEG-PLA NS. NS prepared with polymers containing BGE (1 and 2 mol%) showed similar emission intensities at AlClPc
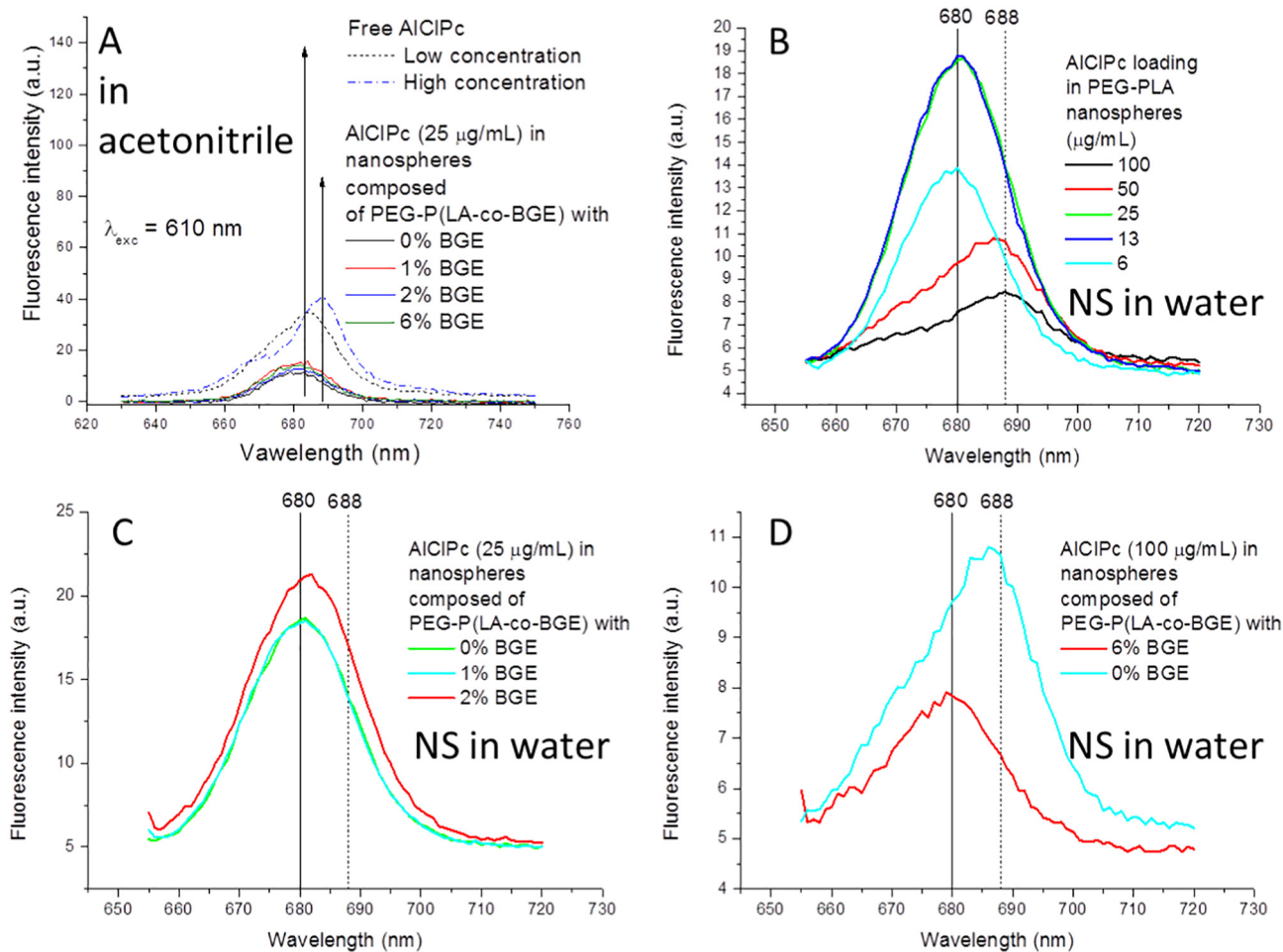
Fig. 10. Fluorescence spectra of chloroaluminum phthalocyanine (AlClPc)-loaded nanospheres (NS) in acetonitrile (A) and in water (B and C). The values in μg/mL refer to AlClPc loading in the original NS formulation, which was further diluted (1:10 in 10 mM aqueous NaCl) for fluorescence measurements. Emission spectra were recorded with 650 nm excitation wavelength, unless otherwise indicated.

loadings of 25 μg/mL (Fig. 10C). At a higher loading of 100 μg/mL, the fluorescence intensity was higher in PEG-PLA NS than in NS prepared from PEG-P(LA-co-BGE₆%) (Fig. 10D). The fluorescence data are thus in agreement with the UV–Vis absorption data in the sense that a decrease in the absorption at 676 nm correlates with fluorescence quenching. While the UV–Vis absorption only decreases when AlClPc is present in the form of molecular aggregates, fluorescence emission may decrease in intensity or suffer quenching due to do several phenomena, including i) a lower chromophore concentration due to lower dye encapsulation, whereby part of the dye is not encapsulated in the NS matrix and does not contribute to either absorption or emission; ii) aggregation-induced fluorescence quenching, whereby part of the encapsulated dye absorbs light at a higher wavelength but does not contribute to fluorescence; iii) concentration-induced self-quenching, whereby higher dye concentration within the NS as a consequence of a higher dye encapsulation efficiency would result in higher quenching, among others. In the latter case the molecularly dispersed dye contributes to both absorption and emission, however reabsorption of the emitted photons produces a bathochromic shift in emission wavelength and lower fluorescence intensity.

3.4. AlClPc release studies

AF4-MALS-FLD fractionation was used to further probe the aggregation state of AlClPc within the NS and stability of the dye loading, encapsulation and release studies were performed as well as kinetics of the photophysical properties in cell culture medium containing fetal bovine serum (FBS) proteins. AF4 is particularly useful to characterize the fluorescence of the dye within a nanocarrier because it allows removal of potentially non-encapsulated dye from nanoscale objects in a formulation without preliminary sample preparation. For this the

separation channel was lined with a 5 kg/mol cut-off membrane, which removes the soluble fraction of the dye, and the nanometric-sized fraction of the sample retained in the separation channel (typically a few nm to 700 nm) and eluted according to their diffusion coefficient [42]. This allowed us to incubate the dye in NS suspension in cell culture medium containing serum proteins, obtain a good separation between the proteins and the NS, and identify the contribution of each fraction to the total sample fluorescence (Fig. 11). The analyses we performed on NS with AlClPc loaded at 25 μg/mL because of their prolonged colloidal stability compared to higher loading, unless otherwise indicated.

Stronger fluorescence was obtained with PEG-PLA NS compared to NS from BGE-containing polymers (Fig. 11A). This result is in agreement with the UV–Vis absorption data obtained in batch mode, which indicate a better dispersion of AlClPc in PEG-PLA NS. In contrast to batch measurements (Fig. 10B), an increase in fluorescence emission with dye concentration was observed in PEG-PLA NS in the whole 6–100 μg/mL concentration range, suggesting that inter-particle filter effect may have contributed to the fluorescence quenching observed in batch measurements. Dye loading had an effect on the size-distribution of the NS and at higher values (25 and 100 μg/mL), whereby PEG-PLA NS presented a significant fraction of larger NS than at lower loadings (Fig. 11B), suggesting that the dye contributed to particle aggregation or particle enlargement due to Oswald ripening. As the larger particle population was not detected at 37 °C in DMEM/FBS (Fig. 11C), it was most likely composed of thermally reversible aggregates or the incubation medium may have contributed to preventing particle aggregation. This also suggests that the BGE containing NS loaded with AlClPc could be suitable for use in biological media containing serum proteins, even though they had limited stability in water.

We studied the release of AlClPc from the NS in aqueous medium by
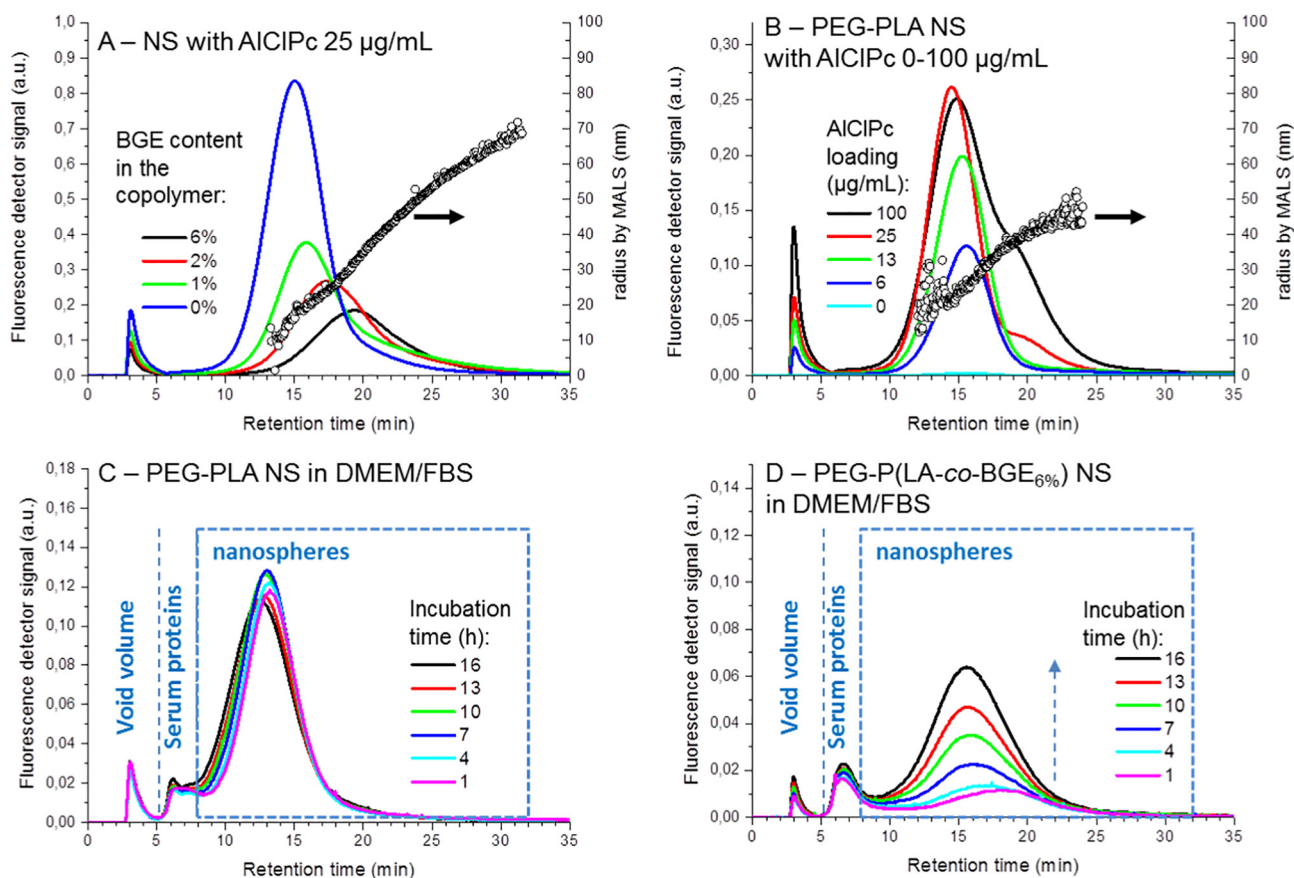
Fig. 11. Fluorescence emission of the nanospheres fractionated by AF4-MALS-FLD. Fractograms obtained with fluorescence detection in NaCl 10 mM at 25 °C (A and B) and dye release in cell culture medium supplemented with fetal bovine serum, at 37 °C (C and D). AlClPc loading was 25 μg/mL unless indicated otherwise.

monitoring the fluorescence emission as a function of time after diluting the NS in NaCl 10 mM at 25 °C, or 37 °C (results not shown), or in DMEM/FBS at 37 °C (Fig. 11C and D). The last set of conditions was selected for their similarities to in vitro conditions for cell culture studies. In addition, serum proteins, including the most ubiquitous serum albumin, offer hydrophobic pockets for the solubilization of lipophilic compounds and are therefore good acceptors to increase the release rate and prevent precipitation of the hydrophobic payload [43,44]. The fluorescence emission of PEG-PLA NS did not vary significantly for up to 16 h under the conditions tested (Fig. 11C). In addition, very little fluorescence was associated to the serum proteins, which elution occurs at retention times between 5 and 10 min. Together these results suggest limited dye release in aqueous medium even in the presence of serum proteins. In PEG-P(LA-co-BGE$_{6\%}$) NS an increase in fluorescence was observed only at 37 °C and in DMEM/FBS (Fig. 11D). This somehow counter-intuitive result can be explained by considering that as the dye escapes the NS, the concentration within the NS decreases, thus self-quenching, due to the inner filter effect or quenching due to aggregation, decreases. This result therefore suggests that the lower fluorescence intensity obtained with PEG-P(LA-co-BGE$_{6\%}$) NS compared to PEG-PLA NS was due to quenching within the NS and not to failure to encapsulate the dye, in agreement with the high encapsulation efficiency of all NS (> 98% by HPLC-FLD). As various factors interfere with the fluorescence emission intensity of AlClPc, this method was found to be unreliable to quantify the release of this specific dye from the NS and further release and encapsulation studies were carried out via HPLC-FLD.

3.5. AlClPc release from the NS in n-octanol

The external sink method [45] is used to study the release of poorly water-soluble compounds from nanocarriers, where sink conditions cannot be reached experimentally in aqueous medium. This is the case of AlClPc, which solubility is < 0.4 μg/mL in phosphate buffered saline (pH 7.4) at 37 °C [24]. By offering high solubility of the encapsulated compound and low solubility of the nanocarrier components n-octanol serves as an external sink, mimicking a cell-membrane capable of receiving the hydrophobic payload as it is released in aqueous medium or present at the nanoparticle interface.

NS composed of PEG-P(LA-co-BGE) with 0, 2 and 6% BGE had low initial rates of AlClPc release and a sigmoidal release profile (Fig. 12). Significant differences in the amount of released dye between the NS were observed from 360 min, indicating higher release rates in the order PEG-PLA > PEG-P(LA-co-BGE$_{2\%}$) > PEG-P(LA-co-BGE$_{6\%}$). The
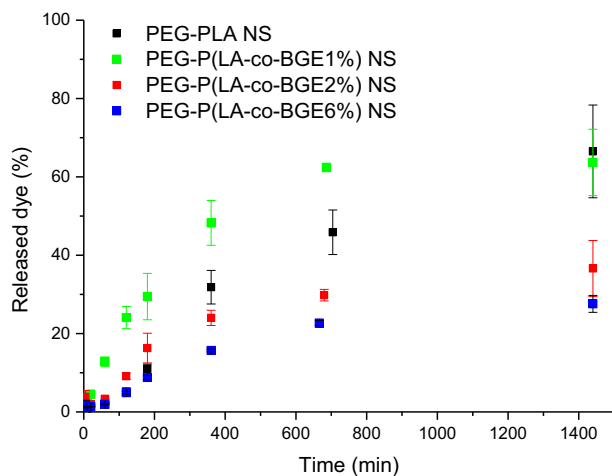

Fig. 12. Chloroaluminum phthalocyanine release from the nanospheres (NS) in *n-octanol* at 37 °C. The NS had 25 μg of AlClPc and 10 mg polymer per mL. The results are means of three experiments ± SD.

NS size may have played a significant role in prolonging the release of AlClPc from the NS, as the dye has to cross the polymer matrix to reach the nanoparticle interface. A significantly higher initial release rate was obtained for the NS composed of PEG-P(LA-co-BGE) with 1% BGE, and the % of released dye followed a logarithmic profile as a function of time. The origin of these discrepancies with respect to the other three NS has not been identified. It is possible that more than one parameter played opposing roles in the release of AlClPc from the NS. For instance, at low BGE content, an increase in the polymer free volume (decrease in T_g) could accelerate drug release, while too little enthalpy gain through aromatic interactions between the dye and the benzyl groups would be insufficient to delay its release. At higher BGE content, the interaction between the dye and the benzyl group on the polymer would counteract the increase in chain mobility and thus delay the release. After a short release time (30 min) the amount of AlClPc released from any of the NS studied here (1 to 6%) was lower than from 115 nm Pluronic® F68-stabilized PLA NS (10%) [5], suggesting that the dense PEG corona at the NS interface may have initially delayed the release and transfer of the dye from the polymeric NS core to the receptor *n-octanol* phase. At 1440 min, however, all pegylated NS had released a higher fraction of the initial dye (28–66%) than from the PLA NS (22%) [5], and NS with the lower BGE content or no BGE had a higher AlClPc release % (66 and 64%, respectively) than PLA nanocapsules or a Pluronic® F68-stabilized nanoemulsion with average particle size of 133 nm (53%) [24]. Therefore, the presence of an oily core in the nanocarrier can be a strategy for sustained release, whereas in a fully polymeric matrix the polymer composition can be selected to tune the release profile.

These preliminary results raise expectations that the polymers studied here could provide nanocarriers with tunable release rates depending on the amount of BGE in hydrophobic block. Due to the short-lived stability in aqueous medium some adjustments would have to be made to prevent nanoparticle aggregation and precipitation and we suggest that one option would be a longer PEG block or higher PEG to P(LA-co-BGE) ratio to counteract the increase in hydrophobicity of the core-forming block due to BGE incorporation.

3.6. Cytotoxicity of the polymers in NS form on J774.A1 macrophage and Vero cell-lines

AlClPc has been found to show cytotoxicity under laser-light activation but also in some cases, to a lesser extent, in the dark [6]. To strictly investigate the safety of the polymers prepared in this work in nanostructure form without interference of loaded dye, blank NS were assayed on J774A.1 macrophages and on Vero cells, a phagocytic and a non-phagocytic cell line, respectively (Fig. 13). Cell viability of 70% is generally used as a threshold below which a tested compound is no longer considered safe. As cytotoxicity is typically a concentration-dependent phenomenon our NS were tested over a concentration range of 10 to 1000 μg/mL. The viability of cells incubated with PEG-PLA NS did not decrease below 70% up to the highest tested concentration in the macrophage cell line, whereas in Vero cells the higher concentration showed a decrease in cell viability to 50%. All NS from BGE containing copolymers maintained the cell viability to values higher than 70% in Vero cells and no significant differences with PEG-PLA NS were found in J774A.1 cells. Therefore, the polymers prepared in this study produce NS that can be considered safe in vitro towards both cell lines.

4. Conclusions

This study enables us to revisit and complement literature data regarding the photo-physical properties of encapsulated phthalocyanine dyes and possible aromatic donor-acceptor interactions with polymeric nanocarriers. In the present study the PLA block in PEG-PLA copolymer is already capable of forming a kinetically frozen matrix that traps and stabilizes AlClPc in its monomeric dispersed state. Substitution of a few LA units by BGE could not increase the already quantitative dye
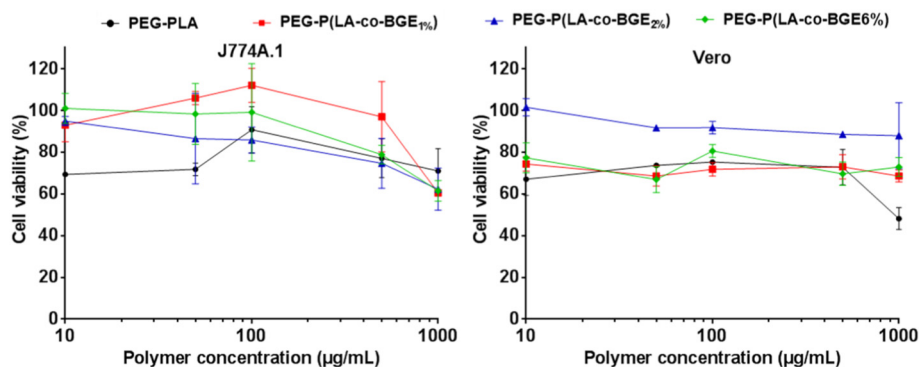
Fig. 13. Viability assay of J774.1 and Vero cell lines incubated with blank nanospheres.

encapsulation and had a detrimental effect on dye dispersion, resulting in dimerization or aggregation of the dye and a subsequent loss of the fluorescence efficiency, but was able to slow down the rate of dye release from the NS. In contrast, other studies involving micelle-forming copolymers with short hydrophobic segments suggest that aromatic substituents increase fluorescence of the dye due to a higher dye encapsulation efficiency, as a consequence of π-π interactions and/or an increase in polymer hydrophobicity. The prolonged colloidal stability, high encapsulation efficiency, sustained release profile and the superior photo-physical properties of the encapsulated dye in PEG-PLA NS identifies it as a promising candidate for photosensitizer nanocarriers in photodynamic therapy with AlClPc. In contrast, for aromatic dyes, photosensitizers or drugs that are not easily encapsulated in PEG-PLA NS, the presence of benzyl groups in PEG-P(LA-*co*-BGE) could improve the drug encapsulation efficiency through π-π interactions, and experiments are in progress to further test this hypothesis.

Author contributions

The manuscript was written through contributions of all authors. All authors have given approval to the final version of the manuscript.

Funding sources

Declarations of interest

None.

Acknowledgment

Appendix A. Supplementary data

Additional GPC data and log P calculations. Supplementary data associated with this article can be found in the online version, at https://doi.org/10.1016/j.msec.2018.09.022.

References

[1] J.P. Figueiro Longo, S.P. Lozzi, A.R. Simioni, P.C. Morais, A.C. Tedesco, R.B. Azevedo, Photodynamic therapy with aluminum-chloro-phtalocyanine induces necrosis and vascular damage in mice tongue tumors, J. Photochem. Photobiol. B. Biol. 94 (2) (2009) 143–146.

[2] K. Liu, X. Wang, V. Ntziachristos, S. Marsch, P. Hunziker, Polymeric nanosystems for near-infrared multispectral photoacoustic imaging: synthesis, characterization and in vivo evaluation, Eur. Polym. J. 88 (2017) 713–723.

[3] D.K. Chatterjee, L.S. Fong, Y. Zhang, Nanoparticles in photodynamic therapy: an emerging paradigm, Adv. Drug Deliv. Rev. 60 (15) (2008) 1627–1637.

[4] L.T. Oliveira, G.M. Garcia, E.K. Kano, A.C. Tedesco, V.C.F. Mosqueira, HPLC-FLD methods to quantify chloroaluminum phthalocyanine in nanoparticles, plasma and tissue: application in pharmacokinetic and biodistribution studies, J. Pharm. Biomed. Anal. 56 (1) (2011) 70–77.

[5] C.S. de Paula, A.C. Tedesco, F.L. Primo, J.M.C. Vilela, M.S. Andrade, V.C.F. Mosqueira, Chloroaluminium phthalocyanine polymeric nanoparticles as photosensitisers: Photophysical and physicochemical characterisation, release and phototoxicity in vitro, Eur. J. Pharm. Sci. 49 (3) (2013) 371–381.

[6] M.P. Siqueira-Moura, F.L. Primo, E.M. Espreafico, A.C. Tedesco, Development, characterization, and photocytotoxicity assessment on human melanoma of chloroaluminum phthalocyanine nanocapsules, Mater. Sci. Eng. C Mater. Biol. Appl. 33 (3) (2013) 1744–1752.

[7] K.R. Py-Daniel, J.S. Namban, L.R. de Andrade, P.E.N. de Souza, L.G. Paterno, R.B. Azevedo, M.A.G. Soler, Highly efficient photodynamic therapy colloidal system based on chloroaluminum phthalocyanine/pluronic micelles, Eur. J. Pharm. Biopharm. 103 (Supplement C) (2016) 23–31.

[8] H. Asem, A. Abd El-Fattah, N. Nafee, Y. Zhao, L. Khalil, M. Muhammed, M. Hassan, S. Kandil, Development and biodistribution of a theranostic aluminum phthalocyanine nanophotosensitizer, Photodiagn. Photodyn. Ther. 13 (2016) 48–57.

[9] I.R. Calori, A.C. Tedesco, Lipid vesicles loading aluminum phthalocyanine chloride: formulation properties and disaggregation upon intracellular delivery, J. Photochem. Photobiol. B. Biol. 160 (2016) 240–247.

[10] G.B. Rodrigues, F.L. Primo, A.C. Tedesco, G.U.L. Braga, In vitro photodynamic inactivation of *Cryptococcus neoformans* melanized cells with chloroaluminum phthalocyanine nanoemulsion, Photochem. Photobiol. 88 (2) (2012) 440–447.

[11] P.L. Goto, M.P. Siqueira-Moura, A.C. Tedesco, Application of aluminum chloride phthalocyanine-loaded solid lipid nanoparticles for photodynamic inactivation of melanoma cells, Int. J. Pharm. 518 (1–2) (2017) 228–241.

[12] B.H. Vilsinski, A.P. Gerola, J.A. Enumo, K.d.S.S. Campanholi, P.C.d.S. Pereira, G. Braga, N. Hioka, E. Kimura, A.L. Tessaro, W. Caetano, Formulation of aluminum chloride phthalocyanine in Pluronic™ P-123 and F-127 block copolymer micelles: photophysical properties and photodynamic inactivation of microorganisms, Photochem. Photobiol. 91 (3) (2015) 518–525.

[13] Y. Yi, G. Lin, S. Chen, J. Liu, H. Zhang, P. Mi, Polyester micelles for drug delivery and cancer theranostics: current achievements, progresses and future perspectives, Mater. Sci. Eng. C 83 (2018) 218–232.

[14] C.K. McLaughlin, J. Logie, M.S. Shoichet, Core and corona modifications for the design of polymeric micelle drug-delivery systems, Isr. J. Chem. 53 (9/10) (2013) 670–679.

[15] J. Ding, L. Chen, L. Xiao, L. Chen, X. Zhuang, X. Chen, Noncovalent interaction-assisted polymeric micelles for controlled drug delivery, Chem. Commun. 50 (77) (2014) 11274–11290.

[16] H. Türk, A. Shukla, P.C. Alves Rodrigues, H. Rehage, R. Haag, Water-soluble dendritic core–shell-type architectures based on polyglycerol for solubilization of hydrophobic drugs, Chem. Eur. J. 13 (15) (2007) 4187–4196.

[17] B. Kulkarni, B. Surnar, M. Jayakannan, Dual functional nanocarrier for cellular

imaging and drug delivery in cancer cells based on pi-conjugated core and biodegradable polymer arms, Biomacromolecules 17 (3) (2016) 1004–1016.

[18] Y. Shi, M.J. van Steenbergen, E.A. Teunissen, L.s. Novo, S. Gradmann, M. Baldus, C.F. van Nostrum, W.E. Hennink, Π–Π stacking increases the stability and loading capacity of thermosensitive polymeric micelles for chemotherapeutic drugs, Biomacromolecules 14 (6) (2013) 1826–1837.

[19] Y. Shi, A. Elkhabaz, F.A.Y. Yengej, J. van den Dikkenberg, W.E. Hennink, C.F. van Nostrum, pi-pi stacking induced enhanced molecular solubilization, singlet oxygen production, and retention of a photosensitizer loaded in thermosensitive polymeric micelles, Adv. Healthc. Mater. 3 (12) (2014) 2023–2031.

[20] E. Lepeltier, C. Bourgaux, P. Couvreur, Nanoprecipitation and the "ouzo effect": application to drug delivery devices, Adv. Drug Deliv. Rev. 71 (2014) 86–97.

[21] Y.E. Aguirre-Chagala, J.L. Santos, R. Herrera-Najera, M. Herrera-Alonso, Organocatalytic copolymerization of a cyclic carbonate bearing protected 2,2-bis (hydroxymethyl) groups and D,L-lactide. Effect of hydrophobic block chemistry on nanoparticle properties, Macromolecules 46 (15) (2013) 5871–5881.

[22] Z. Zhu, Effects of amphiphilic diblock copolymer on drug nanoparticle formation and stability, Biomaterials 34 (38) (2013) 10238–10248.

[23] G. Pound-Lana, J.-M. Rabanel, P. Hildgen, V.C.F. Mosqueira, Functional polylactide via ring-opening copolymerisation with allyl, benzyl and propargyl glycidyl ethers, Eur. Polym. J. 90 (2017) 344–353.

[24] L.T. Oliveira, M.A. de Paula, B.M. Roatt, G.M. Garcia, L.S.B. Silva, A.B. Reis, C.S. de Paula, J.M.C. Vilela, M.S. Andrade, G. Pound-Lana, V.C.F. Mosqueira, Impact of dose and surface features on plasmatic and liver concentrations of biodegradable polymeric nanocapsules, Eur. J. Pharm. Sci. 105 (2017) 19–32.

[25] T. Mosmann, Rapid colorimetric assay for cellular growth and survival - application to proliferation and cytotoxicity assays, J. Immunol. Methods 65 (1–2) (1983) 55–63.

[26] J.L. Espartero, I. Rashkov, S.M. Li, N. Manolova, M. Vert, NMR analysis of low molecular weight poly(lactic acid)s, Macromolecules 29 (10) (1996) 3535–3539.

[27] W.-L. Chen, Y.-F. Peng, S.-K. Chiang, M.-H. Huang, Thermal properties and physicochemical behavior in aqueous solution of pyrene-labeled poly(ethylene glycol)-polylactide conjugate, Int. J. Nanomedicine 10 (2015) 2815–2822.

[28] S. Solarski, M. Ferreira, E. Devaux, Characterization of the thermal properties of PLA fibers by modulated differential scanning calorimetry, Polymer 46 (25) (2005) 11187–11192.

[29] J. Hilf, A. Phillips, H. Frey, Poly(carbonate) copolymers with a tailored number of hydroxyl groups from glycidyl ethers and CO_2, Polym. Chem. 5 (3) (2014) 814–818.

[30] H. Fessi, F. Puisieux, J.P. Devissaguet, N. Ammoury, S. Benita, Nanocapsule formation by interfacial polymer deposition following solvent displacement, Int. J. Pharm. 55 (1) (1989) R1–R4.

[31] R. Gref, G. Miralles, É. Dellacherie, Polyoxyethylene-coated nanospheres: effect of coating on zeta potential and phagocytosis, Polym. Int. 48 (4) (1999) 251–256.

[32] C.R. Heald, S. Stolnik, K.S. Kujawinski, C. De Matteis, M.C. Garnett, L. Illum, S.S. Davis, S.C. Purkiss, R.J. Barlow, P.R. Gellert, Poly(lactic acid)-poly(ethylene oxide) (PLA-PEG) nanoparticles: NMR studies of the central solidlike PLA core and the liquid PEG corona, Langmuir 18 (9) (2002) 3669–3675.

[33] T. Riley, S. Stolnik, C.R. Heald, C.D. Xiong, M.C. Garnett, L. Illum, S.S. Davis, S.C. Purkiss, R.J. Barlow, P.R. Gellert, Physicochemical evaluation of nanoparticles assembled from poly(lactic acid)-poly(ethylene glycol) (PLA-PEG) block copolymers as drug delivery vehicles, Langmuir 17 (11) (2001) 3168–3174.

[34] T. Riley, T. Govender, S. Stolnik, C.D. Xiong, M.C. Garnett, L. Illum, S.S. Davis, Colloidal stability and drug incorporation aspects of micellar-like PLA-PEG nanoparticles, Colloids Surf. B Biointerfaces 16 (1–4) (1999) 147–159.

[35] R. Gref, M. Luck, P. Quellec, M. Marchand, E. Dellacherie, S. Harnisch, T. Blunk, R.H. Muller, 'Stealth' corona-core nanoparticles surface modified by polyethylene glycol (PEG): influences of the corona (PEG chain length and surface density) and of the core composition on phagocytic uptake and plasma protein adsorption, Colloids Surf. B Biointerfaces 18 (3–4) (2000) 301–313.

[36] S.M. D'Addio, W. Saad, S.M. Ansell, J.J. Squiers, D.H. Adamson, M. Herrera-Alonso, A.R. Wohl, T.R. Hoye, C.W. Macosko, L.D. Mayer, C. Vauthier, R.K. Prud'homme, Effects of block copolymer properties on nanocarrier protection from in vivo clearance, J. Control. Release 162 (1) (2012) 208–217.

[37] J.-M. Rabanel, P. Hildgen, X. Banquy, Assessment of PEG on polymeric particles surface, a key step in drug carrier translation, J. Control. Release 185 (2014) 71–87.

[38] M. C., Calculation of Molecular Properties and Bioactivity Score, http://www.molinspiration.com/cgi-bin/properties, (2017), Accessed date: 3 November 2017.

[39] B.H. Vilsinski, A.P. Gerola, E.O. Lemos, P.M. Barbosa, K.S.S. Campanholi, G.B. Cesar, A.L. Tessaro, N. Hioka, W. Caetano, Spectroscopic study of aluminum phthalocyanine chloride (AlPcCl) in homogeneous and micro-heterogeneous media consisting of P-123 and F-127 polymeric micelles, Quim. Nova 38 (5) (2015) (631-U190).

[40] C.C. Jayme, I.R. Calori, A.C. Tedesco, Spectroscopic analysis of aluminum chloride phthalocyanine in binary water/ethanol systems for the design of a new drug delivery system for photodynamic therapy cancer treatment, Spectrochim. Acta A Mol. Biomol. Spectrosc. 153 (2016) 178–183.

[41] P.P. Pompa, G. Ciccarella, J. Spadavecchia, R. Cingolani, G. Vasapollo, R. Rinaldi, Spectroscopic investigation of inner filter effects by phthalocyanine solutions, J. Photochem. Photobiol. A Chem. 163 (1) (2004) 113–120.

[42] A. Zattoni, B. Roda, F. Borghi, V. Marassi, P. Reschiglian, Flow field-flow fractionation for the analysis of nanoparticles used in drug delivery, J. Pharm. Biomed. Anal. 87 (0) (2014) 53–61.

[43] B. Magenheim, M.Y. Levy, S. Benita, A new in vitro technique for the evaluation of drug release profile from colloidal carriers - ultrafiltration technique at low pressure, Int. J. Pharm. 94 (1) (1993) 115–123.

[44] K.S. Soppimath, T.M. Aminabhavi, A.R. Kulkarni, W.E. Rudzinski, Biodegradable polymeric nanoparticles as drug delivery devices, J. Control. Release 70 (1–2) (2001) 1–20.

[45] M. Chorny, I. Fishbein, H.D. Danenberg, G. Golomb, Study of the drug release mechanism from tyrphostin AG-1295-loaded nanospheres by in situ and external sink methods, J. Control. Release 83 (3) (2002) 401–414.